Cell

Dynamics between Stem Cells, Niche, and Progeny in the Hair Follicle

Ya-Chieh Hsu,[1] H. Amalia Pasolli,[1] and Elaine Fuchs[1,*]
[1]Howard Hughes Medical Institute, Laboratory of Mammalian Cell Biology & Development, The Rockefeller University, New York, NY 10065, USA
*Correspondence: fuchslb@rockefeller.edu
DOI 10.1016/j.cell.2010.11.049

SUMMARY

Here, we exploit the hair follicle to define the point at which stem cells (SCs) become irreversibly committed along a differentiation lineage. Employing histone and nucleotide double-pulse-chase and lineage tracing, we show that the early SC descendents en route to becoming transit-amplifying cells retain stemness and slow-cycling properties and home back to the bulge niche when hair growth stops. These become the primary SCs for the next hair cycle, whereas initial bulge SCs become reserves for injury. Proliferating descendents further en route irreversibly lose their stemness, although they retain many SC markers and survive, unlike their transit-amplifying progeny. Remarkably, these progeny also home back to the bulge. Combining purification and gene expression analysis with differential ablation and functional experiments, we define critical functions for these non-SC niche residents and unveil the intriguing concept that an irreversibly committed cell in an SC lineage can become an essential contributor to the niche microenvironment.

INTRODUCTION

Adult stem cells (SCs) govern tissue homeostasis and wound repair. They reside in a specific niche, defined as the microenviroment, that hosts and maintains SCs (Spradling et al., 2008). Most SCs are infrequently cycling, a feature thought to preserve their stemness, namely their ability to self-renew and remain undifferentiated over the animal's lifetime. During normal homeostasis, they often exit from their niches and progress to become transit-amplifying (TA) cells, undergoing a series of rapid divisions before committing to terminal differentiation (Fuchs, 2009; Morrison and Kimble, 2006).

Determining the point in a lineage hierarchy where SCs lose long-term self-renewing capacity and become irreversibly committed represents a fundamental and challenging question in SC biology. Transitioning from a slow-cycling to more fast-cycling state is not indicative, as hematopoietic stem cells (HSCs) and hair follicle (HF) SCs can reversibly switch from dormancy to cycling during normal homeostasis and wound repair (Blanpain et al., 2004; Foudi et al., 2009; Nowak et al., 2008; Taylor et al., 2000; Waghmare et al., 2008; Wilson et al., 2008). Merely exiting their niche is also not a reliable measure, as some HSCs circulate, trafficking between their bone marrow niche and extramedullary tissues (Cao et al., 2004). Even embarking along a differentiation pathway may not be an unequivocal indicator of loss of stemness; studies in *Drosophila* and mouse testis show that germline SC niche vacancies can be filled by early spermatogonial cells that dedifferentiate when returned to the niche (Brawley and Matunis, 2004; Kai and Spradling, 2004; Brinster and Avarbock, 1994).

The murine HF offers an excellent system for monitoring an SC lineage and exploring plasticity of SC progenies. During homeostasis, the lower HF cycles through bouts of active hair growth (anagen), destruction (catagen), and rest (telogen) (Lavker et al., 2003; Paus and Cotsarelis, 1999). When the new HF emerges, it grows next to the old hair, which persists into the next cycle. This creates a protrusion or "bulge," first described >100 years ago (Unna, 1876). In 1990, nucleotide pulse-chase experiments revealed the existence of slow-cycling, label-retaining cells (LRCs) in the bulge (Cotsarelis et al., 1990). A decade later, these cells were isolated, characterized, and shown to self-renew long-term and contribute to HF lineages and wound repair (Blanpain et al., 2004; Claudinot et al., 2005; Ito et al., 2005; Morris et al., 2004; Tumbar et al., 2004; Zhang et al., 2009). These findings established the bulge as a bona fide HF-SC niche.

Hair growth is fueled by bulge SCs, which are activated at the start of anagen by the dermal papilla (DP), a cluster of underlying mesenchymal cells. Upon activation, SCs exit the bulge and proliferate downward, creating a long linear trail of cells, the outer root sheath (ORS) (Ito et al., 2005; Zhang et al., 2009). In mature HFs, the ORS extends from bulge to matrix. Enveloping the DP at the HF base, matrix cells cycle rapidly but transiently before differentiating upward to generate the hair and its channel (Figure 1A and Figure S1A available online).

Catagen illuminates an unambiguous distinction between long-lived HF-SCs and short-lived matrix progeny that undergo massive apoptosis. The remaining epithelial strand retracts, drawing the DP upward. Current evidence suggests that at the catagen/telogen transition, a few bulge SCs migrate to meet the DP, generating the hair germ (HG) (Ito et al., 2004; Zhang et al., 2009). Bearing closer resemblance to bulge than matrix, HG cells are activated prior to bulge at the start of anagen (Greco et al., 2009). Prior to activation, HF-SCs undergo an extended rest period that can last for months.

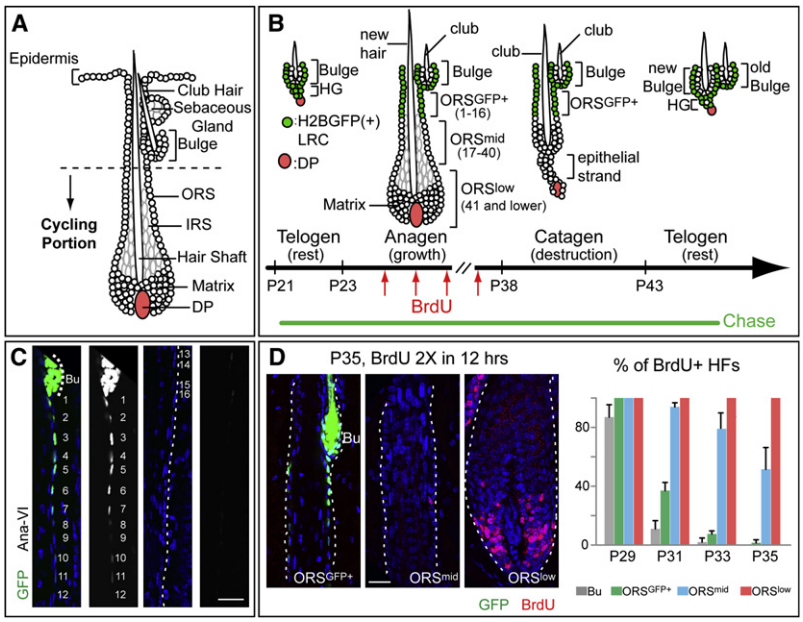

Figure 1. Dynamics of Slow- and Fast-Cycling Cells throughout the Hair Cycle

(A) Cycling portions of a mature HF. (B–D) *Tet-Off H2BGFP* mice were chased from P21 to the days/stages noted (P35–P37 corresponds to AnaVI). Before harvesting skin, some mice were given 2×6 hr pulses of BrdU. Schematic depicts H2BGFP cells (green) that will be label-retaining (LRCs) when the chase is stopped at each stage. Cell #s are counting down from the bulge base (= 0). In (C), the right panels of each pair are duplicates of GFP monochromes of the left panels. Scale bars, 30 μm. Bu, bulge. DAPI in blue. In (D), note that S phase cells in AnaVI are mainly in ORS^{low} and matrix. %HFs with BrdU^{+} cells in bulge or in different ORS segments were quantified from P29–P35. For each stage, n = 2 mice and ≥23 HFs/mouse were counted. Data are mean ± standard deviation SD.

Whereas extensive studies have been performed on bulge SCs and TA-matrix cells, the properties and fates of ORS cells are less clear. Although these cells do not express high levels of CD34, a marker of their SC bulge predecessors, they display many HF-SC markers not found in matrix, including Lgr5, Sox9, Lhx2, and TCF3 (Fuchs, 2009). To date, functional studies on ORS cells have been limited to cultures of microdissected rat whisker HFs, where long-term clones capable of engraftment were obtained not only from bulge and ORS but also from matrix (Claudinot et al., 2005; Oshima et al., 2001; Rochat et al., 1994). Whether ORS cells in vivo possess stemness like their predecessors or are committed like their TA progeny remains unknown.

The unique regenerative aspects of HF homeostasis and the transient, but spatially and temporally well-defined ORS offer an unparalleled opportunity to examine the transition between a SC and a TA cell. Where does the transition from slow cycling to fast cycling occur along the ORS trail? What happens to ORS cells during catagen? Do they undergo apoptosis like TA cells, or do they survive like SCs? If they survive, do they home back to the bulge, and if they do so, do they function as SCs?

Answering these questions could provide fundamental insights into defining not only the importance of bulge to SC survival but also the point where an SC loses its stemness and embarks upon a terminal differentiation pathway. If all ORS cells either die or differentiate during catagen, this would imply that HF-SCs lose stemness once they leave the bulge. If on the other hand, some ORS cells survive and return back to the bulge as functional SCs, this would imply that at least at some point along the progression from bulge to TA compartments, an SC that has left the bulge still possesses intrinsic features of stemness.

In this report, we address these key questions in the unperturbed in vivo confines of the normal hair cycle, as well as in response to injury. In so doing, we unearth surprising and dynamic features of the HF-SC niche and its progeny. First, we show that during anagen, the upper ORS cells remain slow cycling, like their SC predecessors, whereas lower ORS cells cycle more rapidly. Moreover, slow-cycling ORS cells survive catagen and contribute mightily to both HG and a new bulge: in fact, they become the main source of SCs used during the next hair cycle. Lacking a DP, the initial bulge ceases to play a major role in homeostasis but can respond to injury. Finally and perhaps most surprisingly, some actively cycling lower ORS cells not only survive catagen but also home back to the bulge. Like their upper ORS predecessors, these cells retain many HF-SC markers. However, they irreversibly lose their ability to proliferate in normal homeostasis or upon wounding. Instead, they function decisively in hair anchorage during the resting phase and in providing the quiescent signaling cues that control the hair cycle. Our findings define a point along the ORS where cells lose stemness and become irreversibly fated to differentiate or die and illuminate how downstream SC progeny can provide negative feedback to the niche and restrict SC self-renewal and tissue formation.

RESULTS

Bulge Descendents in Anagen ORS Can Be Subdivided into Slow Cycling and Faster Cycling

To dissect the properties of bulge SC descendents along the ORS, we first addressed whether these cells remain slow-cycling like bulge or become faster-cycling like matrix. We used bi-transgenic mice expressing Doxycycline (Doxy)-repressible histone H2BGFP controlled by a *keratin 5* (*K5*) promoter. With this Tet-Off system, skin epithelium is uniformly labeled until Doxy exposure, when new H2BGFP synthesis is tightly repressed and cells deplete existing GFP by 2×/division (Tumbar et al., 2004).

Doxy chase was begun at postnatal day (P)21, just before the start of the 1st hair cycle (Figure 1B). At the last stage of anagen (AnaVI, based on Muller-Rover et al., 2001; P35–P37 in these mice), the bulge but not matrix contained bright H2BGFP LRCs (Figures 1C and 1D). Interestingly, an LRC trail extended from the bulge base along the ORS. To quantify, we standardized image acquisition for GFP intensities by setting the detector so

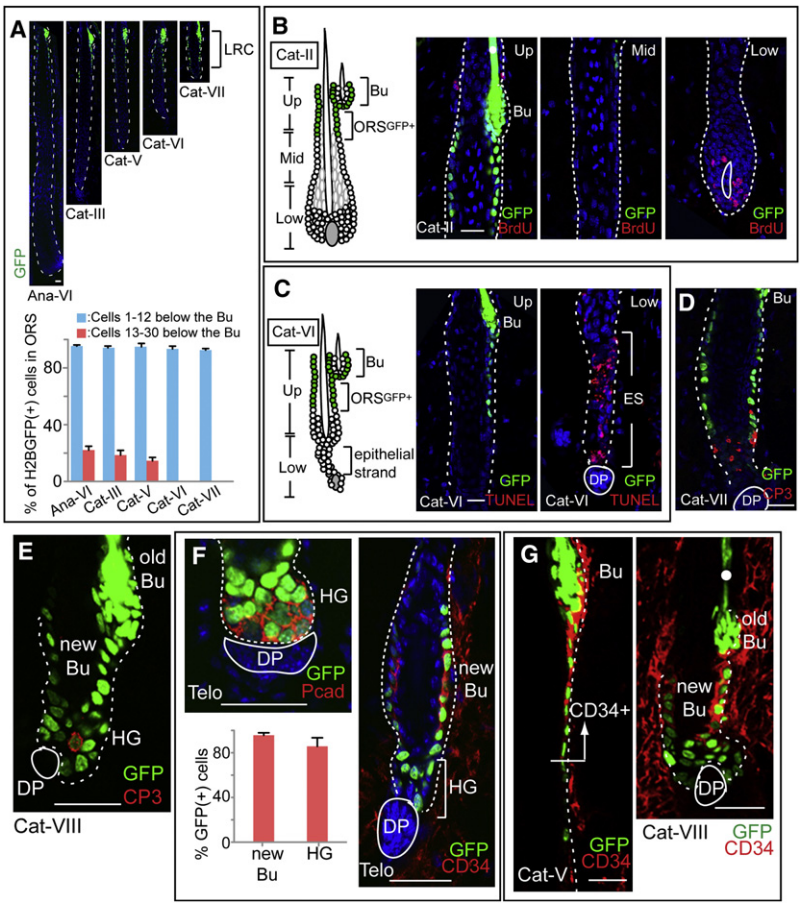

Figure 2. Label-Retaining HF-SC Descendents in the ORS Are Spared from Apoptosis during Catagen and Form a New Bulge and HG at Telogen

Tet-Off H2BGFP mice were chased from P21 to the HF stages indicated. Prior to analysis, some mice were given a 4 hr BrdU pulse.

(A) H2BGFP LRCs maintain the same distribution from anagen VI to catagen's end.

(B) BrdU labeling in early catagen (Cat-II) shows proliferation only in matrix and ORS^{low} and not ORS^{GFP+} or ORS^{mid}.

(C–E) TUNEL and CP3 immunolabeling in catagen VI–VIII reveals cell death in the retracting epithelial strand (ES) but rarely in LRCs.

(F) Fate of H2BGFP LRCs at catagen to 2nd telogen transition. Like the old bulge, the emerging new bulge and HG contain LRCs. Quantifications: n = 3 mice; 42 total HFs analyzed for bulge; 87 for HG.

(G) HF-SC bulge marker CD34 is upregulated in upper ORS^{GFP+} beginning at catagen V. The shape of the future new bulge and HG can already be distinguished at Cat VIII. HFs are outlined by dotted white line. White dots mark autofluorescent hair shafts.

Scale bars, 30 μm. Data are mean ± SD.

that brightest bulge cells were maximal but not saturated in a 12 bit (= 4096 shades) image. Under this condition, bulge was composed almost exclusively of cells with GFP intensities >256 (GFP^{bright}). Within the first 16 positions counting down along the ORS trail in a planar section, >85% of cells were GFP$^+$ (intensity > 16) with the majority of GFP^{bright} cells in #1–12. By contrast, few ORS cells in sites 16–30 were GFP$^+$, and below #30, GFP was not detected (Figure 1C and Figure S1B).

To further probe proliferation heterogeneities during anagen, we performed a series of short BrdU pulse experiments in *Tet-Off H2BGFP* mice. When labelings were conducted at intervals between P27 and P29, i.e., after HFs displayed an emerging inner root sheath (IRS) and typical anagen shape, BrdU$^+$ cells were detected in bulge, ORS, and matrix. By P31, however, most bulge cells had ceased proliferation. Although occasional BrdU$^+$ cells were still seen in ORS positions 1–16, proliferation was mostly beneath this zone in ORS and matrix. By P33, most BrdU$^+$ ORS cells were below #30, and from P35–P37, BrdU$^+$ cells were largely restricted to matrix, with few labeled ORS cells <#40 (Figure 1D and Figure S1C). The transition between ORS and matrix was at ~#75–85.

To summarize: ORS^{GFP+}(#1–16) behaved similarly to bulge, displaying slow-cycling characteristics and returning to quiescence ~2 days after bulge proliferation ceased; ORS^{mid} (#17–40) remained proliferative 2 days after ORS^{GFP+}; and ORS^{low} cells (#40–80) and matrix cycled continuously.

SCs that Exit the Bulge during the Growth Phase and Remain Slow Cycling (ORS^{GFP+}) Are Spared From Apoptosis during the Destructive Phase

Because ORS^{GFP+} cells divide only a few times during anagen, we next wondered what happens to these cells during the destructive phase. Throughout catagen, the ORS^{GFP+} trail showed no signs of migration or expansion (Figure 2A). Three possible lineage behaviors could explain this result: (1) GFP$^+$ ORS cells are static in catagen; (2) the influx of bulge cells to ORS^{GFP+} is compensated by an efflux of ORS^{GFP+} cells, proliferating and moving toward matrix; (3) ORS^{GFP+} cells undergo apoptosis and bulge cells migrate downward to replace them.

To distinguish between these models, we monitored apoptotic and proliferative events during this period. Early catagen was marked by dramatic reduction in matrix proliferation (Figure 2B). Cells within bulge and ORS were mostly quiescent during catagen. These data rule out model 2. Soon thereafter, cell death was detected by DNA fragmentation (TUNEL) and activated caspase 3 (CP3). Apoptosis began within matrix and expanded upward into the retracting epithelial strand (Figure 2C). However, even toward catagen's end, only a few ORS^{GFP+} and bulge LRCs scored positive for TUNEL or CP3, and ultrastructural analysis suggested that these were likely healthy cells that had engulfed apoptotic debris (Figure 2D and Figures S2A–S2D). These data rule out model 3. Together, these differences revealed a striking molecular boundary between the TUNEL/CP3-positive epithelial strand and the apparently unscathed LRCs in bulge and ORS. These data are consistent with model 1.

ORS^{GFP+} Cells Form a New Bulge and Hair Germ at the End of Catagen

As most ORS^{GFP+} cells survive catagen, we next addressed where they go. Near the end of catagen, the LRC trail was still located below the initial bulge. When HFs were followed into telogen and DP adopted its characteristic position directly below the HG, it became apparent that the ORS^{GFP+} trail had adopted a form resembling the HG and a new bulge (Figure 2E).

Imaging and quantifications coupled with fluorescence-activated cell sorting (FACS) analysis confirmed that ~98% of CD34^{+} cells within this new bulge and ~80%–90% of those in HG were GFP^{+} (Figure 2F and Figure S3C). Because in the Tet-Off H2BGFP system, a GFP^{-} cell from an earlier time cannot be the source for a GFP^{+} cell at a later point, this leaves only ORS^{GFP+} and initial bulge as possible sources for this structure.

Given that from catagen to telogen, the initial bulge showed no major change in size or cell number (Figure S2E), our collective evidence favored ORS^{GFP+} as the major source of both this new bulge and HG. These results were surprising, however, because anagen ORS^{GFP+} cells did not show strong immunostaining for either bulge marker CD34 or HG marker P-cadherin. After first confirming that new bulge and HG express these markers (Figure 2F), we traced the temporal roots of these differences. Toward catagen's end, the first ~8 cells in the ORS^{GFP+} zone acquired strong CD34 immunostaining, whereas the lower part of ORS^{GFP+} remained CD34^{-} but became P-cadherin-bright (Figure 2G; data not shown).

To further monitor these events, we performed a lineage-tracing experiment with *Lgr5-EGFP-IRES-CreER/Rosa-stop-LacZ-stop* mice (Barker et al., 2007). At full anagen, Lgr5 was expressed by both bulge and ORS; however, as ORS is >15× larger than bulge, we could preferentially mark ORS cells by giving a low dose of tamoxifen (Figure 3A; Figures S3A and S3B). Indeed when examined by thick sections (90 μm) at anagen's end, >70% of HFs had LacZ^{+} ORS cells, whereas only ~4% had LacZ^{+} bulge cells. When traced into telogen, >20% of HFs had LacZ^{+} cells in new bulge or HG, whereas HFs with LacZ^{+} cells in the old bulge remained at ~5%. These data add to the evidence that ORS^{GFP+} is the main source for both new bulge and HG.

Based upon our proliferation analyses of ORS during anagen, we next began with pulse-chased *Tet-Off H2BGFP* mice and superimposed a series of BrdU pulse-chases that allowed us to differentiate old bulge and ORS^{GFP+} and selectively label different ORS segments. As proliferation within the initial bulge occurs during early anagen (~P25–P29), we preferentially labeled ORS by administering BrdU at P30–P32 (Figure 3B). Moreover, because cells below ORS^{GFP+} cycle frequently, a 6 day chase at anagen's end and into catagen (P38) restricted most BrdU^{+} cells to the ORS^{GFP+} zone. When chased further into telogen, these GFP/BrdU double^{+} cells were found in new bulge and HG, thereby demonstrating that the ORS^{GFP+} of the prior cycle contributes substantially to the new bulge and HG.

Finally, we used epifluorescence intensity analyses to estimate the average number of divisions that GFP^{+} LRCs within each compartment undergo during a hair cycle. Because cell divisions are silenced during catagen and telogen, GFP intensities within each compartment are retained, and thus, their intensities in telogen serve as a guide to their origin nearing anagen's end. Analyses of GFP^{+} cells chased from the start of the first postnatal anagen to telogen revealed that cells that maintained their residence in the initial bulge divided the least (~2×) during the hair cycle: their epifluorescence corresponded to the old bulge (Figure 3C). By contrast, cells that resided in the ORS and acquired CD34 during catagen corresponded in epifluorescence to new bulge and on average divided 1–2× more than the old bulge. LRCs that resided in the ORS, but remained CD34^{-}, displayed epifluorescence corresponding to HG and reflective of ~1–2× more divisions than new bulge. Quantifications in control mice showed that without Doxy, HG and new and old bulges displayed uniform levels of the highest H2BGFP signal, underscoring tight Tet-Off regulation and validating the efficacy of the data (Figure S3C).

Together, these results establish that cells in ORS^{GFP+} are the major source of HG and new bulge. Furthermore, they unveil a hitherto unrecognized relation between HF-SCs that exit the bulge during the growth phase and the new bulge and HG that form during the destructive phase.

Some Mid-Zone ORS Cells Contribute to the HG

The ability of cells within the ORS^{GFP+} to survive catagen led us to wonder whether more fast-cycling bulge progeny located in the middle or lower ORS might also be spared and possibly be the source of the ~10%–20% of HG cells with very low GFP. To test this hypothesis, we delayed our BrdU pulse to P34–P36, a time when most bulge and ORS^{GFP+} cells had ceased proliferation. Although ORS^{mid} cells were proliferative at this time, they became quiescent soon thereafter, as evidenced by their label retention after a 4 day chase. These BrdU^{+} LRCs were uniformly low for GFP and could be found in the HG following a chase into telogen (Figure S3D). Thus although most of the HG was comprised of ORS^{GFP+} cells, the mid-zone was the source of HG cells undergoing the most divisions in the prior hair cycle. This cut-off was further defined by delaying the BrdU pulse so that cells below the mid-zone were preferentially labeled: under these conditions, no BrdU^{+} cells were detected in the HG (see below).

Together, these experiments delineate the ORS^{GFP+} zone as the point at which an HF-SC can exit the initial bulge and still be recycled to the CD34^{+} new bulge. The point at which HF-SCs can be recycled to the HG extends to the mid-zone. Moreover, these data reveal a strong inverse correlation between the number of divisions progeny have undergone and whether they are recycled to bulge versus HG.

A Potential Conundrum: The Return of Some Fast-Cycling Bulge Descendents below the ORS^{mid} Zone to the Niche

During our double-label pulse-chase studies, we noticed that some chased BrdU^{+} cells started to show up in the new bulge when BrdU was pulsed at P34–P36. Their number increased dramatically when the BrdU pulse was delayed to P36–P38 (end of anagen) and then chased through catagen, suggestive that these cells came from a position below the ORS mid-zone (Figure 4A). Closer inspection revealed that in contrast

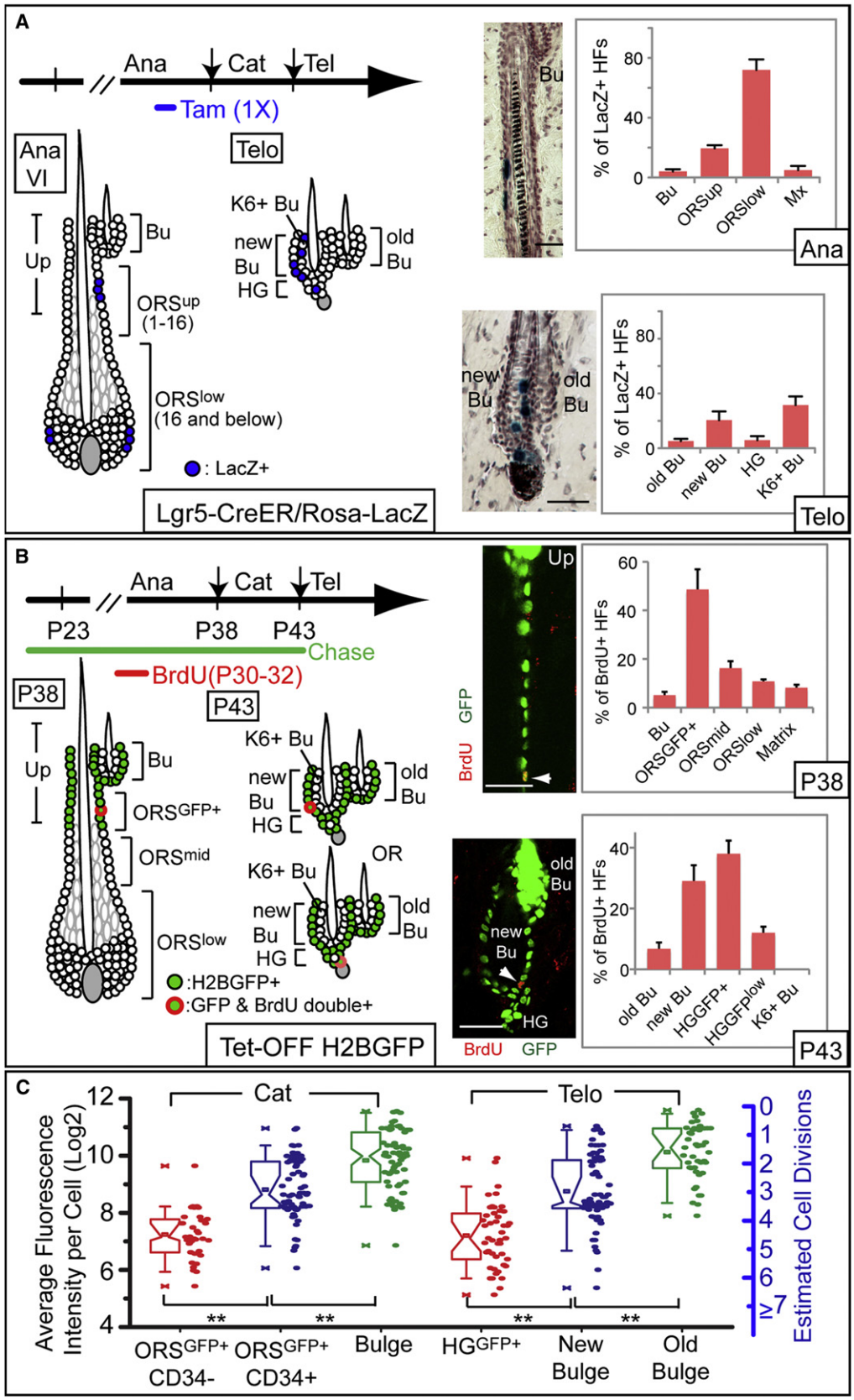
A
Ana
Cat
Tel
Tam (1X)
Ana VI
Telo
Up
Bu
ORSup (1-16)
ORSlow (16 and below)
: LacZ+
Lgr5-CreER/Rosa-LacZ
K6+ Bu
new Bu
HG
old Bu
% of LacZ+ HFs
Bu
ORSup
ORSlow
Mx
Ana
new Bu
old Bu
old Bu
new Bu
HG
K6+ Bu
Telo
B
P23
P38
P43
Chase
BrdU(P30-32)
ORSGFP+
ORSmid
ORSlow
:H2BGFP+
:GFP & BrdU double+
Tet-OFF H2BGFP
Up
GFP
BrdU
% of BrdU+ HFs
Bu
ORSGFP+
ORSmid
ORSlow
Matrix
P38
OR
HG
HGGFP+
HGGFPlow
P43
C
Cat
Telo
Average Fluorescence Intensity per Cell (Log2)
Estimated Cell Divisions
ORSGFP+ CD34-
ORSGFP+ CD34+
Bulge
HGGFP+
New Bulge
Old Bulge

to ORS^{GFP+}, these BrdU$^+$ cells were restricted to the innermost new bulge. Immunolabeling and FACS analysis showed that the cells were CD34$^-$ and hence distinct from suprabasal CD34$^+$ bulge cells described previously (Blanpain et al., 2004). Instead, these cells were positive for keratin 6 (K6) (Figure 4A; Figures S4A–S4C).

K6 is also known to mark the terminally differentiated companion layer, which is derived from matrix during anagen and sandwiched between ORS and IRS (Figure S1A). The K6$^+$ bulge cells differed from companion layer by their expression of key HF-SC transcription factors (Figure 4B). Ultrastructurally, K6$^+$ bulge cells also more closely resembled CD34$^+$ bulge SCs than companion layer cells (Figures S4D–S4F). However, they differed from bulge SCs in making unusual adhesive contacts with the club hair and extensive desmosomal contacts with their neighbors. Thus, the cells fated to enter the innermost layer of the new bulge at the end of catagen were distinct from any of the known HF residents.

The K6$^+$ Bulge Layer Is Derived from Actively Cycling Cells in the Lower ORS

A priori, the K6$^+$ bulge layer could be a bona fide companion layer, derived from matrix but displaying distinct molecular features at different hair cycle stages. Alternatively, it could be derived from actively cycling lower ORS cells, which face a barrier to lineage progression when matrix apoptoses (catagen IV). The latter possibility was intriguing given that the ORS expresses many HF-SC markers that matrix and anagen companion layers do not (Rendl et al., 2005) (Figure S5A).

To identify the source of K6$^+$ bulge cells, we first revisited our *Lgr5-CreER/Rosa-LacZ* lineage tracings, which labeled cells in both upper and lower ORS, but not matrix when induced near the end of anagen (Figure 3A). In telogen, LacZ$^+$ cells were present in both CD34$^+$ and K6$^+$ bulge layers (Figure 3A and Figure S5B). Similar results were obtained when lineage tracings were conducted with *K14creER/Rosa26-LacZ* mice (Figure S5C). Together with the BrdU pulse results, these data suggest that the K6$^+$ bulge layer comes from lower ORS and not matrix.

To further demonstrate that the lower ORS→matrix cell step that occurs during anagen is bypassed in catagen, we used *K14-Tet-On/H2BGFP* mice, which, upon Doxy, turn on H2BGFP in ORS (Nguyen et al., 2006). When Doxy was given at mid-anagen and HFs were examined at anagen's end, H2BGFP was nicely expressed in ORS (including its CD34$^+$ bulge layer) but not matrix or companion layer (Figure 4C). Given that H2BGFP is stable and ORS cells don't divide during catagen, the fate of label could be monitored. Through catagen IV, bright H2BGFP persisted only in ORS. At catagen V after the matrix apoptosed, GFP$^+$ cells appeared in the K6$^+$ layer at the tip of the retracting club hair (shown).

These cells survived catagen, remained K6$^+$ and GFP$^+$, expressed HF-SC/ORS markers, and wound up in the telogen bulge (Figure 4C; Figures S5F and S5G). Moreover, because when chased into telogen, K6$^+$ cells of new bulge were GFP$^+$ whereas those of old bulge were GFP$^-$, the GFP labeling reflected lineage fate mapping and not ectopic *K14* promoter activity (shown). We also confirmed this by inducing *H2BGFP* in telogen and verifying absence of GFP$^+$ cells in the K6$^+$ bulge layer (Figure 4C; Figure S5D). These results exclude both matrix and anagen companion layer as possible precursors of the K6$^+$ bulge. Moreover, the catagen-imposed bypassing of the ORS→matrix transition explains the dramatically different biology between cells of the K6$^+$ bulge (ORS-derived) and companion layer (matrix-derived).

To specifically follow the fate and movement of ORS^{low} cells, we combined a BrdU pulse-chase scheme (pulse at the end of anagen) with this *Tet-On H2BGFP* strategy. ORS^{low} was the only population with BrdU/H2BGFP double$^+$ cells in every HF. As expected, starting from catagen V, double$^+$ cells appeared in the K6$^+$ layer around the newly formed club hair and retracted upward with it as the new bulge formed. During catagen, a few double$^+$ cells also appeared in the epithelial strand and in the external layer flanking newly formed K6$^+$ cells (Figure 4C; Figure S5G). In sharp contrast to these layers, however, no TUNEL$^+$ or CP3$^+$ cells were detected in the ORS-derived K6$^+$ layer (Figure S5E, 0/352 HF examined). Thus, although some ORS^{low} cells survived catagen and wound up in new bulge, they took up residence in the K6$^+$CD34$^-$ layer.

K6$^+$ Bulge Cells Do Not Participate in Normal Homeostasis

We next wondered whether niche environment might restore HF-SC function to lower ORS-derived bulge cells, enabling them to utilize the remaining proliferative capacity they possessed prior to catagen. The importance of testing this possibility was heightened when we discovered that the K6$^+$ layer displayed not only HF-SC markers Sox9, Lhx2, and TCF3, still expressed by lower ORS, but also nuclear NFATc1, previously found only in bulge SCs (Horsley et al., 2008) (Figure S6A).

Figure 3. ORS^{GFP+} LRCs Form the HG and CD34$^+$ SCs of the New Bulge

Schematics summarize experiments and results.

(A) Lineage tracing with *Lgr5CreER/Rosa-LacZ* to monitor ORS cell fate. Tamoxifen was given in full-anagen. Three days later (AnaVI), most HFs had LacZ$^+$ cells in ORS (both up and low) but not bulge or matrix. When chased to telogen, LacZ$^+$ cells showed up mainly in new bulge (both CD34$^+$ and K6$^+$ layers). n = 2 mice, 176 HFs. Quantifications were on 90 μm sections; images shown are 20 μm sections (hematoxylin counterstain).

(B) H2BGFP/BrdU double-label, double-pulse-chase experiment to monitor fate of upper ORS^{GFP} cells. Tet-Off H2BGFP mice were chased from P21 and BrdU pulses during mid-anagen (P30–P32) preferentially labeled cells in the upper ORS^{GFP} trail. When chased to the anagen/catagen transition (P38), many HFs had BrdU$^+$ LRCs in their ORS^{GFP+} (arrowhead); BrdU$^+$ LRCs were rare elsewhere (n = 3 mice, 42 HFs). When chased to telogen (P43), BrdU$^+$/GFP$^+$ cells (arrowhead) were mainly in the new bulge or HG (n = 3 mice, 58 HFs). Scale bars, 30 μm. new Bu and K6$^+$ Bu denote CD34$^+$ and K6$^+$ layers of new bulge.

(C) Relative epifluorescence intensities of cells from different LRC populations of *Tet-Off H2BGFP* mice chased from the 1st telogen through one hair cycle. Raw datasets are plotted to right of each box-and-whisker diagram: median, 25th and 75th percentiles are denoted by notch, bottom and top boxes; 5th and 95th percentile are whiskers; minimum and maximum measurements are x's. Asterisks indicate significant differences between datasets (**p < 0.01). Data are mean ± SD.

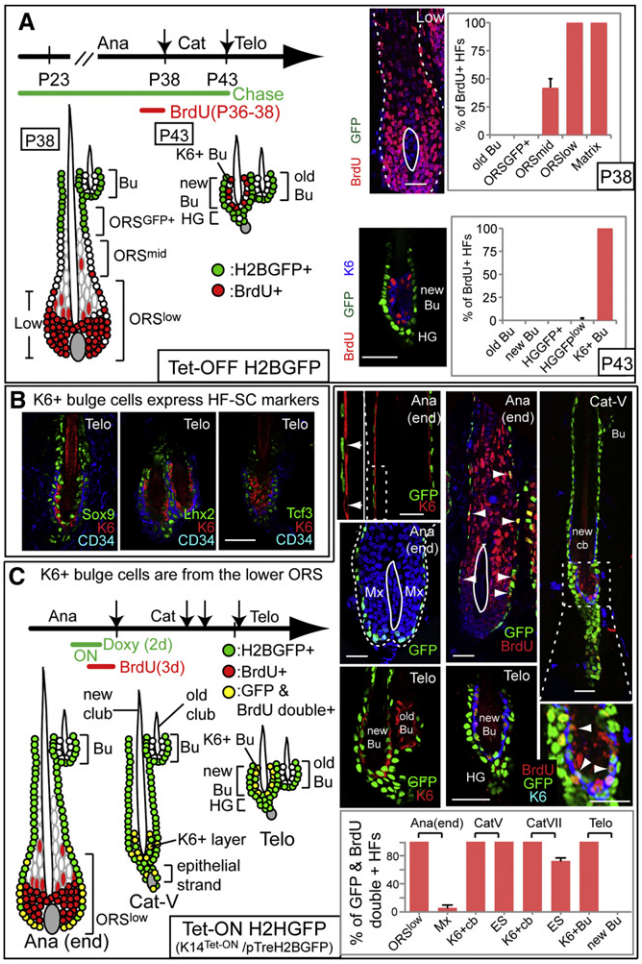

Figure 4. K6⁺ Bulge Cells Express HF-SC Markers and Are Derived from Actively Cycling Lower ORS during Catagen

(A) H2BGFP/BrdU double-label, double pulse-chase scheme to monitor fate of cells below the mid-zone ORS. BrdU was administered to Tet-Off H2BGFP mice at anagen's end (P36–P38) and analyzed directly, or after chasing to telogen. At P38, many lower ORS and matrix cells are BrdU⁺ (n = 2 mice, 38 HFs). When chased to P43, BrdU⁺ LRCs are restricted to the K6⁺ layer of the new bulge (n = 4 mice, 129 HFs).

(B) K6⁺ bulge cells express key transcription factors characteristic of bulge SCs and their ORS progeny.

(C) Lineage tracing with *K14Tet-On/H2BGFP* coupled with BrdU pulse-chase. Doxy was administered to turn on H2BGFP in the entire ORS, but not K6⁺ companion layer or matrix, in late anagen. From catagen V through telogen, H2BGFP is detected in K6⁺ cells at the tip of the newly formed club hair. This layer retracts with the club hair during catagen and winds up in the new bulge by telogen. Note that K6⁺ old bulge cells are not GFP⁺. If BrdU is given at anagen's end, BrdU⁺/H2BGFP⁺ cells are found in ORS^{low}. At catagen, double⁺ cells are in the K6⁺ layer, which by telogen has moved inside new bulge.

Scale bars, 30 μm. K6⁺ club = K6⁺ layer enclosing new club hair. new Bu and K6⁺ Bu denote CD34⁺ and K6⁺ layers of new bulge (n = 2 mice; >23 HFs per stage). Data are mean ± SD.

We first addressed whether K6⁺ bulge cells proliferate in the next hair cycle. To capture proliferation if it existed, we pulsed with BrdU throughout the 2 day window of early anagen when HF-SCs are most active. Under conditions where >60% of CD34⁺ bulge cells incorporated BrdU, no proliferation was detected in K6⁺ bulge cells of >190 HFs examined (Figure 5A).

Although the K6⁺ bulge layer was quiescent, it was possible that some of its cells might migrate to the CD34⁺ layer or ORS and contribute to the hair cycle. We ruled this out by administering BrdU at the end of anagen and then chasing into telogen to selectively label K6⁺ bulge cells (Figure 5B). When chased throughout the following hair cycle, no migration of BrdU-labeled cells was observed. In the next telogen, BrdU label remained within the K6⁺ layer of what became the old bulge (Figure 5B; Figure S6B).

Our data infer that even though highly proliferative cells in anagen can wind up in the bulge, slow-cycling CD34⁺ cells are the source of new HFs. To further substantiate this, we took *Tet-Off H2BGFP* mice that were chased from P21 to the 2nd telogen, so that H2BGFP labeled CD34⁺ old and new bulge and CD34⁻ HG but not K6⁺ bulge cells or HF cells above the bulge (Figure 5C). When the 2nd adult anagen began, the emerging follicle was composed of GFP⁺ cells. Even though proliferation rapidly diluted out label, the fluorescence intensity was still higher than all other HF compartments except CD34⁺ bulge and HG. Thus although prior lineage tracings have shown contributions of CD34⁺ bulge and HG cells to the new HF (Morris et al., 2004; Zhang et al., 2009), these new data further suggest that cells in the K6⁺ bulge layer, junctional zone, sebaceous gland, and infundibulum do not contribute to normal HF homeostasis. Based upon these data, CD34⁺ slow-cycling SCs appear to be the sole source of SCs used for HF homeostasis.

CD34⁺ HF-SCs in Both Old and New Bulge Participate in Wound Repair, whereas K6⁺ Bulge Cells Do Not Respond to Either Wounding or CD34⁺ Bulge Cell Ablation

The new HF always emerged from new and not old bulge, leading us to wonder whether the old bulge functions in normal homeostasis. Careful inspection revealed an occasional proliferative cell at the base of the old bulge, but only when BrdU was pulsed at anagen III, i.e., the height of new bulge activity (Figure 6A). However, when quantified, this constituted <15% of combined bulge activity, indicating that the CD34⁺ new bulge is primarily responsible for fueling new HF downgrowth.

CD34⁺ bulge cells are known to contribute to wound repair (Blanpain et al., 2004; Ito et al., 2005; Morris et al., 2004). Two additional questions now surfaced: (1) As the old bulge still contains CD34⁺ HF-SCs, does it contribute to wound repair, and if so, does it do so equivalently with the new bulge? (2) While refractile to normal homeostasis, do K6⁺ bulge cells participate in wound repair?

To address these questions, we introduced punch wounds during the extended 2nd telogen, administered BrdU, and then examined the skin 2 days later (Figure 6B). BrdU⁺ cells were found in the CD34⁺ outer layer of new bulge and its associated HG. Proliferating CD34⁺ cells were also detected in old bulge. Quantifications revealed similar contributions from the bulges, but only from CD34⁺ and not K6⁺ cells.

Next, we tested responses under more extreme conditions: HF-SC ablation (Figure 6C). *K15-CrePGR* mice were used to induce expression of *d*iphtheria *t*oxin *r*eceptors (DTRs) (Buch et al., 2005) in CD34⁺ bulge cells. RU486 was given to activate CrePGR, followed by DT to ablate CD34⁺ bulge cells. Activated

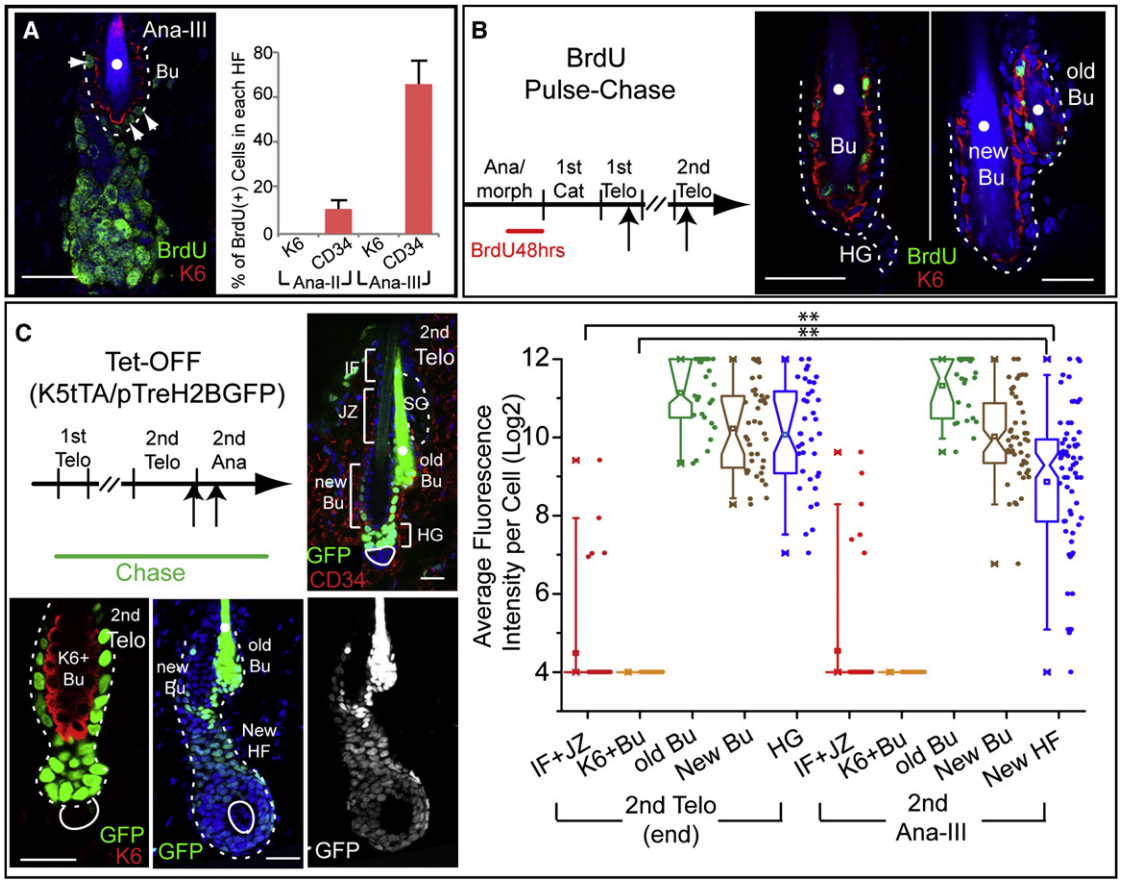

Figure 5. CD34$^+$ Bulge SCs and HG Are the Only Cells Used in Normal HF Homeostasis

(A) Representative example and quantifications of HFs in early anagen (AnaII–AnaIII) with 2 day BrdU pulse. Note BrdU in some CD34$^+$ HF-SCs (arrowheads) but not inner K6$^+$ bulge cells. White dots denote autofluorescent club hair (n = 2 mice, 61 HFs for AnaII; n = 3 mice, 133 HFs for AnaIII).

(B) A 2 day BrdU pulse given at anagen's end is followed through two hair cycles. Although not proliferative, K6$^+$ bulge cells retain label from late anagen predecessors. K6$^+$/BrdU$^+$ cells persist through the next hair cycle and become the K6 layer of old bulge.

(C) Lineage tracing using Tet-Off H2BGFP mice shows that the new HF comes from bulge LRCs. Chase was begun at 1st telogen; analysis began at end of 2nd telogen when H2BGFP selectively labels old bulge, new bulge, and HG. Developing HFs are composed solely of H2BGFP$^+$ cells. IF, infundibulum; JZ, junctional zone; SG, sebaceous gland. Scale bars, 30 μm. Box-and-whisker plots measure H2BGFP epifluorescence intensity within different HF populations. Note paucity of GFP intensity in IF, JZ, and K6$^+$ bulge, revealing their lack of contribution to GFP$^+$ newly forming HF.

**$p < 0.01$. Data are mean ± SD.

CP3 was prevalent in CD34$^+$ but not K6$^+$ bulge layers, verifying selective targeting. Death was equivalent for both new and old bulges, and a 2 day BrdU pulse prior to analyses further revealed proliferation in CD34$^+$ bulge cells that had not been ablated (Figure 6C; data not shown). By contrast, K6$^+$ bulge cells did not respond even when the HF-SC reservoir was depleted.

K6$^+$ Bulge Cells Fail to Grow In Vitro

To address K6$^+$ bulge cell potential, we devised a strategy to isolate them by FACS and then carried out colony formation assays (Figure 6D). An *Lhx2-GFP* transgene behaved similarly to endogenous Lhx2, displaying GFP in both K6$^+$ and CD34$^+$ bulge layers of telogen HFs (Figure S6C). K6$^+$ and CD34$^+$ cells in the GFP$^+$ pool were then further fractionated by differential CD34, E-cadherin, and integrin levels: K6$^+$ bulge cells were gated as GFP$^+$CD34$^-$α6$^-$β1$^-$Ecad^{high}, whereas CD34$^+$ cells were sorted as GFP$^+$ and CD34$^+$. Post-sort marker analysis revealed >94% purity, and consistent with immunofluorescence, RT-PCR showed that K6$^+$ and CD34$^+$ cells expressed similar levels of *Sox9, Lhx2, Tcf3*, and *Nfatc1* (Figures S6C and S6D). In vitro, even though both populations attached to their substratum, only CD34$^+$ and not K6$^+$ bulge cells formed colonies (Figure 6D). Collectively, these data suggest that lower ORS cells that home back to the bulge have irreversibly lost their proliferative and regenerative potential.

K6$^+$ Bulge Cells Function to Retain the Hair Coat and Maintain HF-SC Quiescence

If K6$^+$ bulge cells do not function as HF-SCs, what are their functions in the bulge niche? The first clues came from hair-plucking studies (Figure S7A). When telogen hairs were plucked, the entire K6 layer came with the club hair, demonstrating a tight association. By contrast, most CD34$^+$ cells remained in the bulge.

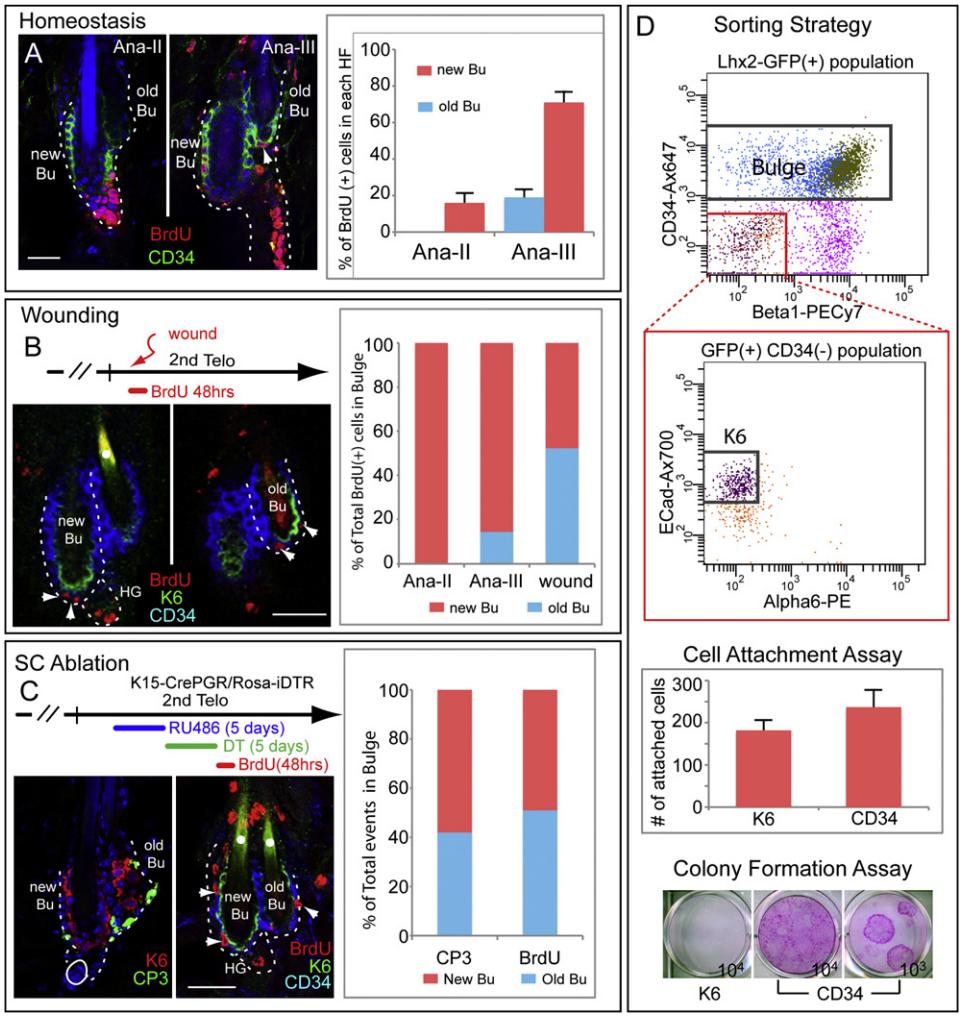

Figure 6. CD34$^+$ but Not K6$^+$ Bulge Cells Are Activated in Wound Repair and upon HF-SC Ablation

(A) Homeostasis. Mice given a 2 day pulse with BrdU at start of 2nd anagen were monitored to AnaIII. Arrowhead marks BrdU$^+$ cell in old bulge, which is >3× less active than new bulge (n = 3 mice, 62 HFs).

(B) Wounding. Punch biopsies were from 2nd telogen. BrdU given over 2 days shows that old and new bulges participate comparably in injury responses (n = 3 mice, 31 HFs).

(C) SC ablation. *K15-CrePGR* was used to express DTR in CD34$^+$ bulge during 2nd telogen. After DT and BrdU, mice were analyzed (n = 3 mice, 64 HFs). Note that when bulge SCs are ablated, remaining CD34$^+$ cells from old and new bulges proliferate, whereas K6$^+$ bulge cells are refractory. Scale bars, 30 μm.

(D) K6$^+$ and CD34$^+$ bulge cells were isolated by FACS from telogen HFs of *Lhx2-EGFP* mice and subjected to culture experiments, performed in triplicate. One thousand cells of each population were assayed for attachment 16 hr post-plating. K6$^+$ and CD34$^+$ cells were also plated, and at 3 weeks, colonies were fixed and stained with 1% Rhodamine B.

Data are mean ± SD.

To test whether the K6$^+$ layer functions to anchor the club hair to the bulge, we devised a strategy to preferentially ablate K6$^+$ versus CD34$^+$ bulge cells (Figure 7A). *Sox9-CreER* (Soeda et al., 2010) is expressed in both K6$^+$ and CD34$^+$ bulge layers. However, in *Sox9-CreER/Rosa-iDTR* mice, when hairs were first trimmed and tamoxifen was applied topically, drug entered the hair pores and preferentially induced DTR in K6$^+$ cells. By contrast, RU486 induced DTR in CD34$^+$ bulge cells of *K15-CrePGR/Rosa-iDTR* mice (Figure 7D and data not shown). Following DTR induction, mice were then treated with DT. Within 4 days, *Sox9-iDTR* mice began to show hair loss and by day (D) 6 the coat was gone (Figure 7B; 5 of 5 mice tested). During this time, *K15-iDTR* mice kept their hair coat even when slightly more bulge cells were ablated (Figure S7B).

Interestingly, 2 days after hair loss, skins of *Sox9-iDTR* mice became dark (Figure 7B). This indicator of anagen entry (Muller-Rover et al., 2001) was substantiated by histological analyses (shown). It occurred ≥50 days earlier than in *K15-iDTR* or control mice (Figure 7C). By mechanisms unknown, hair plucking also triggers anagen reentry. Interestingly, *Sox9-iDTR* mice were >4 days quicker to enter anagen compared to mice undergoing hair plucking, but K6$^+$ bulge cells were

also lost by plucking (Figure S7A). These collective findings led us to consider the possibility that it is loss of K6$^+$ bulge that triggers this precocious anagen. We therefore assessed whether K6$^+$ bulge cells actively participate in maintaining telogen.

To focus specifically on the effects of K6$^+$ cell loss rather than hair loss or mechanical trauma, we identified conditions wherein sufficient K6$^+$ bulge cells survived in our *Sox9-iDTR* mice so that club hairs were retained longer. We then adjusted RU486 so that total bulge cell death events were similar between *Sox9-* and *K15-iDTR* mice (Figure S7B). Under these conditions, CP3$^+$ cells were detected in CD34$^+$ (*K15-iDTR*) and K6$^+$ (*Sox9-iDTR*) layers beginning at D2, peaking at ~D4–D6 and waning by D10 (Figure 7D; data not shown).

In *K15-iDTR* mice, apoptosis was accompanied by brief proliferation from surviving CD34$^+$ bulge cells, as detected by sequential BrdU pulses over this interval. This appeared to be a repair response, as HFs thereafter returned to quiescence and anagen was not induced (Figure 7E; Figure S7C). By contrast, despite club hair retention (Figure 7E, inset), *Sox9-iDTR* HFs not only displayed more robust CD34$^+$ proliferation but soon afterwards entered anagen. Throughout these treatments, K6$^+$ cells showed no signs of proliferation. These effects were not observed with RU486, tamoxifen, or DT alone (Figure 7C; data not shown), confirming that K6$^+$ bulge cells contribute markedly in maintaining the resting state of the hair cycle. Intriguingly, the effects of K6$^+$ cell loss were transient: following anagen entry, CD34$^+$ bulge cells gradually returned to quiescence (data not shown).

To explore what potential signals from the K6$^+$ bulge might influence CD34$^+$ cell behavior, we focused on *Fgf18* and *Bmp6.* These genes were previously shown to be upregulated in CD34$^+$ telogen bulge cells in vivo, and their encoded factors inhibit HF-SC cycling in vitro (Blanpain et al., 2004; Greco et al., 2009). Remarkably, purified K6$^+$ bulge cells displayed enormous enrichment of these genes compared to other epidermal or dermal cells that might impact on bulge microenvironment. Moreover, *fgf18* and *bmp6* expression levels were >25× in K6$^+$ versus CD34$^+$ bulge cells (Figure 7F).

To test whether these factors account for the ability of K6$^+$ bulge cells to maintain CD34$^+$ bulge quiescence, we ablated the K6$^+$ layer in *Sox9-iDTR* mice and injected these growth factors intradermally using fluorescent beads as a guiding reference. In contrast to buffer and beads alone, each of these factors potently suppressed CD34$^+$ bulge activation upon ablation of the K6$^+$ layer (Figure 7G; Figure S7D).

DISCUSSION

Recycling SCs Caught in Transit from Their Niche to The TA Compartment

In this study, we examined the fate of HF-SCs that departed from their niche but had not yet reached the TA pool when the destructive phase began. In contrast to the prevailing view, we discovered that many ORS cells in transit between bulge and matrix survive the massive apoptosis that follows anagen. By using H2BGFP as a sensitive and stable label for lineage tracing, we not only tracked the fate of CD34$^+$ HF-SCs but also distinguished descendents on the basis of cell divisions that occur after departing the niche. By combining this powerful approach with classical lineage tracing and nucleotide pulse-chase, we discovered that descendents closest to the bulge and that undergo the fewest cell divisions are recycled and contribute to the long-term SC pool that fuels the subsequent hair cycle. Bulge descendents a little further en route become activated SCs of the HG (Greco et al., 2009). Fast-cycling ORS cells nearer to matrix return to the bulge and function, but not as bona fide SCs (Figure S7F).

Recycled SCs Make a New Niche

It was hitherto unrecognized that HF-SCs that depart their niche in one cycle become CD34$^+$ bulge SCs for the next cycle. Our findings further imply that HF-SCs with fewer divisions are set aside in reserve within the old bulge, whereas those undergoing more divisions are recycled into a new bulge for homeostasis. In this regard, it is intriguing that in hematopoiesis, the most quiescent HSCs participate in injury repair whereas less quiescent ones are used in homeostasis (Foudi et al., 2009; Wilson et al., 2008). It will be interesting in the future to probe deeper into the impact of cell divisions on HF-SC stemness and to explore how melanoblast and other SCs in the bulge migrate and function in this dynamic niche environment.

The Origin of the HG

Two major theories propose how the HG originates: (1) the lateral disc hypothesis posits that the HG comes from *Shh*$^+$ cells within matrix (Panteleyev et al., 2001); and (2) the bulge migration hypothesis suggests that HG cells migrate from the bulge at the catagen/telogen transition (Ito et al., 2004; Zhang et al., 2009). Both models are attractive, and although *Shh*$^+$ matrix cells are not the source of HF-SCs or HG (Greco et al., 2009), we show that cells outside the bulge clearly survive the destructive phase, as initially speculated (Panteleyev et al., 2001). Moreover, our study extends the similarities between HG and bulge (Greco et al., 2009; Ito et al., 2004; Zhang et al., 2009) even though HG appears to be derived from ORS-SCs that exited the bulge during the prior growth phase.

Our findings agree with prior studies emphasizing close proximity to DP stimuli in explaining why HG is activated so quickly at the start of a new cycle (Greco et al., 2009). However, our new data suggest that this enhanced sensitivity may also rely upon the intrinsic feature of having traveled further along the lineage and divided 1–2× more than new bulge cells. Moreover, as the ORS mid-zone is at the nexus along the lineage at which long-term self-renewing potential begins to wane, this could explain why HG cells do not sustain stemness in vitro (Greco et al., 2009).

Unexpected Origins and Properties of the K6$^+$ Bulge: Insights into Hair Cycle Control

Our findings suggest that when catagen is initiated and matrix undergoes apoptosis, proliferative cells in the lower ORS are short-circuited and return to the bulge. This finding helps to resolve the paradox as to why there are fast-cycling cells from anagen that return to the bulge (Jaks et al., 2008). Since these cells do express many HF-SC markers, it is tempting to conclude that they are SCs coming home to roost. However, our data

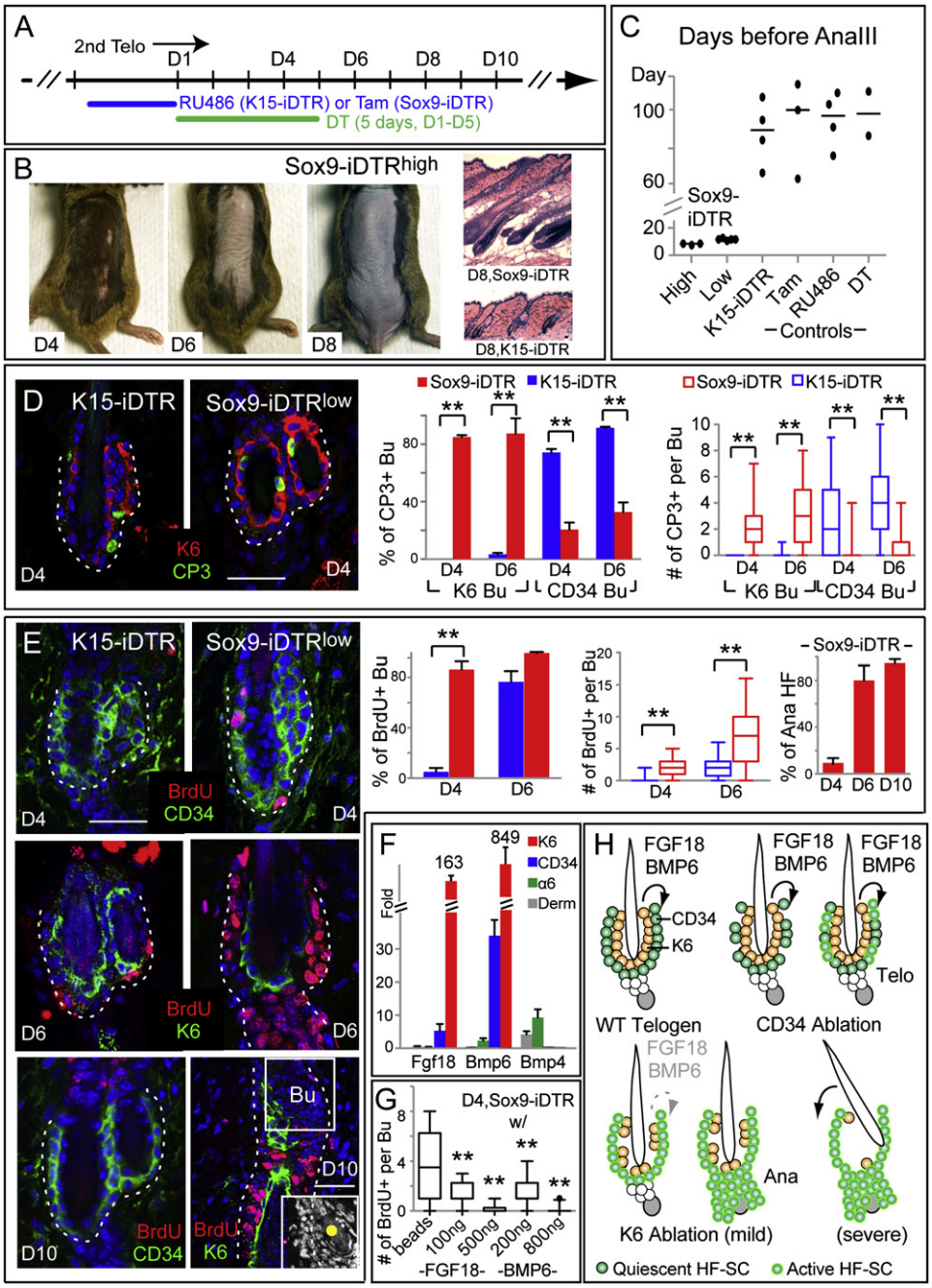

Figure 7. K6$^+$ Bulge Cells Anchor the Club Hair and Serve as a Signaling Center for the HF-SC Niche

(A) Scheme to differentially express DTR in K6$^+$ and CD34$^+$ bulge cells and selectively DT-ablate each layer during extended 2nd telogen. D1 = day 1 of DT injection. Sox9-iDTR^{high} was treated with Tamoxifen for 4 days while Sox9-iDTR^{low} was treated for 2 days (see text).

(B) In contrast to *K15-iDTR* mice, *Sox9-iDTR* mice lose their hair coat at D6 (anchoring function) and skin turns black at D8, reflective of precocious entry into anagen and confirmed by histology.

(C) Quantifications of anagen entry (signaling function). Graph shows #days before HFs entered anagen III for various genotypes/treatments. Horizontal bars denote median.

(D and E) DT-treated *K15-* and *Sox9-iDTR* mice were given a 1 day BrdU pulse at times indicated prior to immunodetection of apoptotic and proliferation markers on skin sections. In D10 Sox9-iDTR image, K6 marks the anagen companion layer. Scale bars, 30 μm. Graphs quantify %bulges positive for CP3, BrdU, and anagen. Box-and-whisker plots indicate #events per HF/bulge: mid-line, median; box, 25th to 75th percentiles; whiskers, minimum and maximum.

(F) Real-time PCR on FACS-isolated populations. Values are normalized to total skin (epidermis+dermis) mRNAs. *Bmp4* is higher in dermis (derm) and α6$^+$ cells as previously reported (Plikus et al., 2008). Note high *Fgf18* and *Bmp6* expression in K6$^+$ bulge cells.

(G) *Sox9-iDTR* mice were treated 3 days with DT and growth factors and then 1 day with BrdU before analysis of proliferation (>24 HFs/experiment in duplicate).

clearly show that once catagen sets in, the proliferative potential of these cells ceases and cannot be reactivated for either homeostasis or wound repair.

The most interesting facet of these surviving lower ORS cells is that despite their failure to regain proliferative potential, they perform essential non-SC functions in the bulge. We posit that their special ability to sense the bulge niche and thereby halt upward protrusion of hair from the skin surface could originate from retention of HF-SC markers when normal lineage progression is bypassed. Additional environmental cues (Figure S7E) along the lineage may endow them with differentiation features that enable their anchorage to the hair shaft and protect the animal against cyclical alopecia.

Perhaps even more remarkable is that lower ORS-derived bulge cells act as a signaling center in the niche (Figure 7H). FGF18 and BMP6 were previously identified as autocrine factors able to maintain bulge SC quiescence (Blanpain et al., 2004; Greco et al., 2009). Our findings confirm these data but also point to a paracrine loop that likely transmits a burst of these key factors to bulge SCs at the catagen/telogen transition when the $K6^+$ layer forms. By imposing potent quiescence signals to the niche, the K6 bulge layer counterbalances the activating role provided by the DP at this time. In this way, the K6 bulge layer establishes the need for prolonged crosstalk between HF-SCs and DP to generate the blocking factors that enable HF-SCs to overcome this threshold (Greco et al., 2009). Moreover, at anagen, the DP moves away from the niche toward the matrix but the K6 layer remains with the bulge, thereby launching a regulatory switch between bulge SCs and TA matrix. We posit that the smaller autocrine FGF18/BMP6 signals may further provide a means for HF-SCs along the upper ORS to retain their slow-cycling status until the new bulge is formed. Our studies now pave the way to test such hypotheses in the future.

Lessons Learned about Stem Cell Biology

By taking advantage of the distinct cycling properties of the HF lineage, we designed unambiguous lineage-tracing experiments to determine the sources and fates of HF-SCs and their descendents throughout homeostasis. By superimposing a temporal series of pulse-chase experiments, we adopted the principles of a movie to monitor HF-SC movement during the hair cycle. This strategy could be useful for many other SCs that display proliferative differences with their progeny.

Although the system has its advantages, the timing of labeling can determine whether the slow-cycling SCs retain the label (e.g., Cotsarelis et al., 1990; Morris and Potten, 1999) or their committed fast-cycling progeny do (e.g., Jaks et al., 2008). Our studies also reveal an example of SC progeny that have become irreversibly committed and yet that still express SC markers and home back to their SC niche. These revelations may help to resolve some controversies that have arisen from label-retaining and conventional lineage-tracing experiments in this and other SC systems.

Several other concepts derived from our study could have broad implications for SC biology: First, our data show that a downstream lineage of SCs can be a critical component of the niche microenvironment and regulate the rate of SC divisions. However, our data also illustrate the power of intrinsic factors on stemness. As exemplified by the $K6^+$ bulge layer and in contrast to the *Drosophila* germline (Brawley and Matunis, 2004; Kai and Spradling, 2004), once cells lose these features, regaining stemness is not assured by returning to an unperturbed niche, nor by depleting the niche of its SCs. Thus, although the niche can markedly affect SC behavior, it may not be sufficient to reset the stemness clock once SCs have passed the point of no return in a lineage. Future studies will be valuable in further defining the distinctions and the parallels among different SCs and their niches.

EXPERIMENTAL PROCEDURES

Mice and Labeling Experiments

Lhx2-EGFP was generated by the GENSAT project (Heintz, 2004). See Extended Experimental Procedures for all other strains used. Tet-Off and Tet-On were activated by continuously feeding mice with Doxy (2 mg/kg) starting at P21 or times specified. CreER was activated by intraperitoneal injection (150 μg/g tamoxifen in corn oil) or topical application (10 mg/ml in ethanol) as specified. CrePGR activation was by topical application of RU486 (1% in ethanol). For 5-Bromo-2′-deoxyuridine (BrdU) pulse-chase experiments, mice were injected intraperitoneally (50 μg/g) (Sigma-Aldrich) and chased for times specified. To test for rare proliferations, injections were supplemented with dietary BrdU water (0.8 mg/ml).

Hair Cycle Timing

Subdivisions of the hair cycle into 6 anagen and 8 catagen stages were based on Muller-Rover et al. (2001). Because hair cycles vary among strains and sexes, stages instead of mouse ages were usually evaluated. For *K5-tTA/pTRE-H2BGFPK5-tTA (Tet-Off)* mice, both are provided. Typically 3–4 mice of matched sex were analyzed.

Wounding and Ablation

0.6 cm punch biopsy wounds were created on backs of anesthetized mice. For ablation of bulge cells, *K15-CrePGR* or *Sox9-CreER X Rosa-iDTR* mice were first treated topically to induce Cre, then injected intraperitoneally (i.p.) with diphtheria toxin (200 ng DT/injection, Sigma) 1×/day for 5 days.

Quantifications of H2BGFP Intensities

Different stages of *Tet-Off H2BGFP* HFs were costained for CD34 and imaged by LSM510 laser-scanning confocal (same laser input and gain). Fluorescence intensities were measured using MetaMorph 7 (Universal Imaging Corp.). Cell division numbers were estimated based on H2BGFP epifluorescence intensity (brightest cells assigned 0 divisions). To reflect cell proliferation histories, native H2BGFP intensities were measured. The exception is Figure 5C where signals were enhanced with GFP antibody and laser input and gain were increased as necessary to detect weakly fluorescent cells. Individual data points were plotted, and statistic analyses (Student's t test) were performed using OriginLab 7.5 or Prism 5 software. Box-and-whisker plots are used to describe the entire population without assumptions on statistical distribution (Schober et al., 2007).

(H) Model summarizes different outcomes of ablating $K6^+$ versus $CD34^+$ bulge cells in telogen. When $CD34^+$ cells are ablated, remaining HF-SCs become activated briefly but then return to quiescence. When $K6^+$ cells are ablated, quiescent signals (FGF18, BMP6) from $K6^+$ bulge are lost, greatly reducing the threshold for anagen activation. The $K6^+$ bulge layer also functions to anchor the club hair.

**$p < 0.01$. Data are mean ± SD.

SUPPLEMENTAL INFORMATION

Supplemental Information includes Extended Experimental Procedures and seven figures and can be found with this article online at doi:10.1016/j.cell.2010.11.049.

ACKNOWLEDGMENTS

We are grateful to colleagues who generously donated mice, especially B. de Crombrugghe (UT MD Anderson) and H. Akiyama (Kyoto University) for sharing *Sox9-CreER* mice prior to publication; S. Mazel, C. Bare, and RU's FCRC for FACS sorting; A. North (Bioimaging Resource Center) for advice in image acquisition; Comparative Biology Center (AAALAC-accredited) for health care to our mice; and members of the Fuchs' lab, in particular: T. Chen, D. Devenport, E. Ezhkova, and B. Keyes for comments on the manuscript; M. Schober for advice on image analyses and quantifications; N. Stokes and D. Oristian for assistance in mouse research. Y.-C. H. is a Starr Stem Cell Scholars Postdoctoral Fellow. This work was supported by grants from NIH (R01AR050452), Starr Foundation, and NYSTEM (N09G074) to E.F., who is an HHMI Investigator. RU FCRC is supported by the Empire State Stem Cell fund through NYSDOH Contract #C023046.

Received: May 3, 2010
Revised: October 1, 2010
Accepted: November 17, 2010
Published: January 6, 2011

REFERENCES

Barker, N., van Es, J.H., Kuipers, J., Kujala, P., van den Born, M., Cozijnsen, M., Haegebarth, A., Korving, J., Begthel, H., Peters, P.J., and Clevers, H. (2007). Identification of stem cells in small intestine and colon by marker gene Lgr5. Nature *449*, 1003–1007.

Blanpain, C., Lowry, W.E., Geoghegan, A., Polak, L., and Fuchs, E. (2004). Self-renewal, multipotency, and the existence of two cell populations within an epithelial stem cell niche. Cell *118*, 635–648.

Brawley, C., and Matunis, E. (2004). Regeneration of male germline stem cells by spermatogonial dedifferentiation in vivo. Science *304*, 1331–1334.

Brinster, R.L., and Avarbock, M.R. (1994). Germline transmission of donor haplotype following spermatogonial transplantation. Proc. Natl. Acad. Sci. USA *91*, 11303–11307.

Buch, T., Heppner, F.L., Tertilt, C., Heinen, T.J., Kremer, M., Wunderlich, F.T., Jung, S., and Waisman, A. (2005). A Cre-inducible diphtheria toxin receptor mediates cell lineage ablation after toxin administration. Nat. Methods *2*, 419–426.

Cao, Y.A., Wagers, A.J., Beilhack, A., Dusich, J., Bachmann, M.H., Negrin, R.S., Weissman, I.L., and Contag, C.H. (2004). Shifting foci of hematopoiesis during reconstitution from single stem cells. Proc. Natl. Acad. Sci. USA *101*, 221–226.

Claudinot, S., Nicolas, M., Oshima, H., Rochat, A., and Barrandon, Y. (2005). Long-term renewal of hair follicles from clonogenic multipotent stem cells. Proc. Natl. Acad. Sci. USA *102*, 14677–14682.

Cotsarelis, G., Sun, T.T., and Lavker, R.M. (1990). Label-retaining cells reside in the bulge area of pilosebaceous unit: implications for follicular stem cells, hair cycle, and skin carcinogenesis. Cell *61*, 1329–1337.

Foudi, A., Hochedlinger, K., Van Buren, D., Schindler, J.W., Jaenisch, R., Carey, V., and Hock, H. (2009). Analysis of histone 2B-GFP retention reveals slowly cycling hematopoietic stem cells. Nat. Biotechnol. *27*, 84–90.

Fuchs, E. (2009). The tortoise and the hair: Slow-cycling cells in the stem cell race. Cell *137*, 811–819.

Greco, V., Chen, T., Rendl, M., Schober, M., Pasolli, H.A., Stokes, N., Dela Cruz-Racelis, J., and Fuchs, E. (2009). A two-step mechanism for stem cell activation during hair regeneration. Cell Stem Cell *4*, 155–169.

Heintz, N. (2004). Gene expression nervous system atlas (GENSAT). Nat. Neurosci. *7*, 483.

Horsley, V., Aliprantis, A.O., Polak, L., Glimcher, L.H., and Fuchs, E. (2008). NFATc1 balances quiescence and proliferation of skin stem cells. Cell *132*, 299–310.

Ito, M., Kizawa, K., Hamada, K., and Cotsarelis, G. (2004). Hair follicle stem cells in the lower bulge form the secondary germ, a biochemically distinct but functionally equivalent progenitor cell population, at the termination of catagen. Differentiation *72*, 548–557.

Ito, M., Liu, Y., Yang, Z., Nguyen, J., Liang, F., Morris, R.J., and Cotsarelis, G. (2005). Stem cells in the hair follicle bulge contribute to wound repair but not to homeostasis of the epidermis. Nat. Med. *11*, 1351–1354.

Jaks, V., Barker, N., Kasper, M., van Es, J.H., Snippert, H.J., Clevers, H., and Toftgard, R. (2008). Lgr5 marks cycling, yet long-lived, hair follicle stem cells. Nat. Genet. *40*, 1291–1299.

Kai, T., and Spradling, A. (2004). Differentiating germ cells can revert into functional stem cells in Drosophila melanogaster ovaries. Nature *428*, 564–569.

Lavker, R.M., Sun, T.T., Oshima, H., Barrandon, Y., Akiyama, M., Ferraris, C., Chevalier, G., Favier, B., Jahoda, C.A., Dhouailly, D., et al. (2003). Hair follicle stem cells. J. Investig. Dermatol. Symp. Proc. *8*, 28–38.

Morris, R.J., and Potten, C.S. (1999). Highly persistent label-retaining cells in the hair follicles of mice and their fate following induction of anagen. J. Invest. Dermatol. *112*, 470–475.

Morris, R.J., Liu, Y., Marles, L., Yang, Z., Trempus, C., Li, S., Lin, J.S., Sawicki, J.A., and Cotsarelis, G. (2004). Capturing and profiling adult hair follicle stem cells. Nat. Biotechnol. *22*, 411–417.

Morrison, S.J., and Kimble, J. (2006). Asymmetric and symmetric stem-cell divisions in development and cancer. Nature *441*, 1068–1074.

Muller-Rover, S., Handjiski, B., van der Veen, C., Eichmuller, S., Foitzik, K., McKay, I.A., Stenn, K.S., and Paus, R. (2001). A comprehensive guide for the accurate classification of murine hair follicles in distinct hair cycle stages. J. Invest. Dermatol. *117*, 3–15.

Nguyen, H., Rendl, M., and Fuchs, E. (2006). Tcf3 governs stem cell features and represses cell fate determination in skin. Cell *127*, 171–183.

Nowak, J.A., Polak, L., Pasolli, H.A., and Fuchs, E. (2008). Hair follicle stem cells are specified and function in early skin morphogenesis. Cell Stem Cell *3*, 33–43.

Oshima, H., Rochat, A., Kedzia, C., Kobayashi, K., and Barrandon, Y. (2001). Morphogenesis and renewal of hair follicles from adult multipotent stem cells. Cell *104*, 233–245.

Panteleyev, A.A., Jahoda, C.A., and Christiano, A.M. (2001). Hair follicle predetermination. J. Cell Sci. *114*, 3419–3431.

Paus, R., and Cotsarelis, G. (1999). The biology of hair follicles. N. Engl. J. Med. *341*, 491–497.

Plikus, M.V., Mayer, J.A., de la Cruz, D., Baker, R.E., Maini, P.K., Maxson, R., and Chuong, C.M. (2008). Cyclic dermal BMP signalling regulates stem cell activation during hair regeneration. Nature *451*, 340–344.

Rendl, M., Lewis, L., and Fuchs, E. (2005). Molecular dissection of mesenchymal-epithelial interactions in the hair follicle. PLoS Biol. *3*, e331.

Rochat, A., Kobayashi, K., and Barrandon, Y. (1994). Location of stem cells of human hair follicles by clonal analysis. Cell *76*, 1063–1073.

Schober, M., Raghavan, S., Nikolova, M., Polak, L., Pasolli, H.A., Beggs, H.E., Reichardt, L.F., and Fuchs, E. (2007). Focal adhesion kinase modulates tension signaling to control actin and focal adhesion dynamics. J. Cell Biol. *176*, 667–680.

Soeda, T., Deng, J.M., de Crombrugghe, B., Behringer, R.R., Nakamura, T., and Akiyama, H. (2010). Sox9-expressing precursors are the cellular origin of the cruciate ligament of the knee joint and the limb tendons. Genesis 10.1002/dvg.20667.

Spradling, A.C., Nystul, T., Lighthouse, D., Morris, L., Fox, D., Cox, R., Tootle, T., Frederick, R., and Skora, A. (2008). Stem cells and their niches: integrated units that maintain Drosophila tissues. Cold Spring Harb. Symp. Quant. Biol. *73*, 49–57.

Taylor, G., Lehrer, M.S., Jensen, P.J., Sun, T.T., and Lavker, R.M. (2000). Involvement of follicular stem cells in forming not only the follicle but also the epidermis. Cell *102*, 451–461.

Tumbar, T., Guasch, G., Greco, V., Blanpain, C., Lowry, W.E., Rendl, M., and Fuchs, E. (2004). Defining the epithelial stem cell niche in skin. Science *303*, 359–363.

Unna, P.G. (1876). Beitrage zur histologie und entwicklungsgeschichte der menschlichen oberhaut und ihrer anhangsgebilde. Arch. Mikroskop. Anat. Entwicklungsmech. *12*, 665–741.

Waghmare, S.K., Bansal, R., Lee, J., Zhang, Y.V., McDermitt, D.J., and Tumbar, T. (2008). Quantitative proliferation dynamics and random chromosome segregation of hair follicle stem cells. EMBO J. *27*, 1309–1320.

Wilson, A., Laurenti, E., Oser, G., van der Wath, R.C., Blanco-Bose, W., Jaworski, M., Offner, S., Dunant, C.F., Eshkind, L., Bockamp, E., et al. (2008). Hematopoietic stem cells reversibly switch from dormancy to self-renewal during homeostasis and repair. Cell *135*, 1118–1129.

Zhang, Y.V., Cheong, J., Ciapurin, N., McDermitt, D.J., and Tumbar, T. (2009). Distinct self-Renewal and differentiation phases in the niche of infrequently dividing hair follicle stem cells. Cell Stem Cell *5*, 267–278.